Substrate Effect on the Plasmon Resonance of Supported Flat Silver Nanoparticles

ARTICLE *in* THE JOURNAL OF PHYSICAL CHEMISTRY C · JANUARY 2011

Impact Factor: 4.77 · DOI: 10.1021/jp1056495 · Source: OAI

4 AUTHORS, INCLUDING:

Yves Borensztein
Pierre and Marie Curie University - Paris 6
106 PUBLICATIONS **1,510** CITATIONS
SEE PROFILE

Cyril Langlois
Institut National des Sciences Appliquées de…
43 PUBLICATIONS **762** CITATIONS
SEE PROFILE

Emmanuelle Lacaze
Pierre and Marie Curie University - Paris 6
92 PUBLICATIONS **1,278** CITATIONS
SEE PROFILE

THE JOURNAL OF PHYSICAL CHEMISTRY C

ARTICLE

pubs.acs.org/JPCC

Substrate Effect on the Plasmon Resonance of Supported Flat Silver Nanoparticles

M. Valamanesh,[†,‡] Y. Borensztein,[*,†] C. Langlois,[‡] and E. Lacaze[*,†]

[†]Institut des NanoSciences de Paris (INSP), CNRS-UMR 7588, UPMC Univ Paris 06, 4 place Jussieu, 75252, Paris Cédex 05, France

[‡]Laboratoire Matériaux et Phénomènes Quantiques, CNRS-UMR 7162, Université Paris Diderot - Paris 7, Bâtiment Condorcet, 10 rue Alice Domon et Léonie Duquet, 75205 Paris Cedex 13, France

ABSTRACT: Substrate effect on the plasmon resonance of flat Ag particles is investigated experimentally, through the comparison between a system with particles on a substrate of amorphous carbon and a system with particles embedded in amorphous carbon. We demonstrate experimentally, in agreement with the theoretical predictions of Bobbert and Vlieger, that the conventional "spherical" dipole approximation fails to reproduce the interaction of the oblate spheroidal particles with the substrate. On the contrary, the use of a so-called "spheroidal" dipole approximation yields a very good agreement with the experiment, leading only to a slight red-shift of the plasmon resonance. Moreover, we show that the shape distribution of the flat particles deposited on the substrate can be successfully extracted from an experimental spectrum within this model.

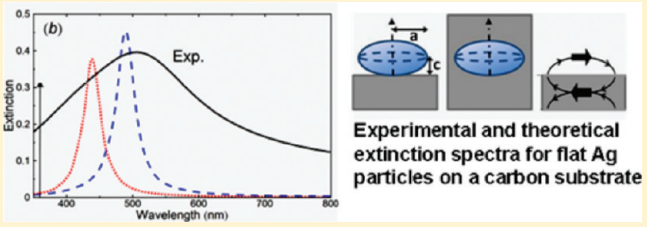

1. INTRODUCTION

Plasmon resonance in metallic nanoparticles (NPs) have received in the last 20 years an exponentially increasing interest, partly because of possible applications in various fields, such as nanophotonics, plasmonics, optoelectronics, optical chemical sensors, biology, and so forth.[1−4] From a theoretical point of view, the understanding of the plasmon resonance in NPs is well documented,[5,6] but theoretical calculations are still challenging in a number of cases, in particular for NPs with irregular shapes[7] or for NPs in interaction, either with other NPs or with a substrate.[8−12] The influence of the substrate and of the dielectric environment for arbitrary shaped NPs has been already numerically demonstrated, although simple analytical approaches are usually not possible.[13] In his pioneering work, Yamaguchi[14] treated the particular case of spheres or ellipsoids in close interaction with a substrate by use of the dipole-image approach within the quasi-static approximation, in order to obtain the local electric field acting on the particle. Every ellipsoidal NP was approximated by a point-dipole in electrostatic interaction with the other NPs on the surface, with its own image-dipole and with the image-dipoles of the other NPs. In the following, this approach will be called the spherical dipole approximation ("spherical DA"). For an isolated particle on the surface, only the interaction with its own image is in play, and it leads in most cases to a red shift of the plasmon resonance. Although this approach has been used, and is still used by many authors,[15−17] it has been shown both theoretically[9,10,18] and experimentally[19,20] that it leads to nonsatisfying results, especially for flat particles: (i) the calculated red shift is much larger than the experimental one, and (ii) it cannot reproduce possible multipolar resonances present beside the dipolar one. Actually, as shown by Vlieger's group[9,18] and other authors,[10,21,22] an exact treatment of this problem, still within the quasi-static approximation, can be done by considering an infinite series of multipolar modes, i.e., of multipolar distributions of charges at the surface of the particle, which fully describes the interaction with the substrate. This multipole method is based on "multipoles located at the center of the particles and 'image multipoles' at the image of this center with respect to the surface of the substrate".[9] The truncation of this infinite series defines the accuracy of the calculation.[10,19,20,23] In the case of flat spheroidal particles, the convergence of the calculation requires very large truncation numbers, which lead to quite heavy calculations. Bobbert and Vlieger[9] have proposed an alternative theoretical approach, in which this *spherical* multipole distribution is replaced by a *spheroidal* multipole distribution, which leads to a much faster convergence.

We show here experimentally that the conventional spherical DA fails in the case of supported flat Ag particles, while the spheroidal dipole approximation (spheroidal DA), which is the first term of the spheroidal multipole distribution, provides good agreement with the experimental results, with little change when the spheroidal quadrupolar order is taken into account. We show also that, even for a flat particle, the effect of the substrate on the optical response of the particle is rather weak. To reach this conclusion, we compare the measured optical response of flat Ag NPs deposited on an amorphous carbon substrate, where the

Received: June 18, 2010
Revised: December 10, 2010
Published: January 28, 2011

interaction with the substrate has to be taken into account, with the same NPs embedded in amorphous carbon where there is no substrate/NP interface.

2. EXPERIMENTAL DETAILS

A semitransparent film of amorphous carbon was first deposited by pulsed laser deposition technique (PLD) onto a microscope glass substrate maintained at 150 °C. Silver NPs were then deposited by PLD onto the amorphous carbon film at the same temperature, with a rate of 1.5 nm nominal thickness per minute measured by means of a quartz microbalance. This procedure led to the formation of Ag NPs whose average size, shape, and distribution on the surface depend on the chosen substrate temperature and deposition rate. Two samples containing the same amount of silver NPs (nominal thickness of 2 nm) were prepared in the same conditions. In the first one, the Ag NPs were left at the surface of the carbon film, while in the second one the NPs were covered by a film of carbon of several tens of nanometers deposited under the same conditions as the substrate film. Elaborated in this way, the only difference between the samples is that the second one contains the particles inside a matrix of carbon, while in the first one the particles are on the surface of carbon.

The morphological characteristics of the first sample were determined by use of an atomic force microscope (AFM). The AFM (Nanoscope Dimension 3100, Veeco Instruments) was used in "tapping mode" to obtain the topography of the surface, using a Si tip with resonance frequency around 300 kHz.

UV−visible transmission spectra T_{sample} of the samples were recorded with a commercial Cary-5 spectrophotometer. The transmission spectra $T_{reference}$ of the slides of glass covered with amorphous carbon films similar to the sample ones were also measured as references. All measurements were performed with the polarization of light aligned parallel to the carbon sample surface. The transmission measurements give the total extinction efficiency of the thin layer of Ag NPs on the surface, defined by the ratio $Q_{ext} = 1 - (T_{sample}/T_{reference})$. For small amounts of Ag NPs (see Figure 4), Q_{ext} is directly given by the total cross section of all NPs, relative to the illuminated sample area.[5]

3. THEORY

3.1. Dielectric Function of Ag NPs. We use in the following the bulk dielectric function of Ag,[24] which we modified in order to take into account the limited size of the Ag NPs, smaller that the electron mean free path of bulk. The modified dielectric function is written as[25,26]

$$\varepsilon_{Ag}^{mod}(\omega) = \varepsilon_{Ag}^{bulk}(\omega) + \frac{\Omega_p{}^2}{\omega(\omega + i\tau_{bulk}{}^{-1})} - \frac{\Omega_p{}^2}{\omega(\omega + i\tau_{mod}{}^{-1})} \quad (1)$$

where

$$\Omega_p = \left(\frac{Ne^2}{\varepsilon_o m}\right)^{1/2} \quad (2)$$

is the Drude plasma frequency of the "free" or conduction s−p electrons in silver, which is the value of the plasma frequency when the screening due to the "bound" electrons, i.e., the effect of the interband transitions, is not taken into account. Here N is the density of conduction electrons, e is their charge, and m is their effective mass. For silver, $\hbar\Omega_p$ can be determined from the experimental dielectric function and is equal to 9.2 eV.[24] τ_{mod} denotes the electronic relaxation time of the free electrons in the Ag NPs, reduced with respect to its value in bulk τ_{bulk} because of the scattering of the conduction electrons at the surface of the NPs, which decreases their mean free path l_{mod} ($= v_{Fermi}\tau_{mod}$). In bulk silver, the mean free path is equal to 43 nm.[24] For Ag nanospheres, the following expression can be used:[5,27]

$$l_{mod}{}^{-1} = l_{bulk}{}^{-1} + \frac{A}{R} \quad (3)$$

where R is the radius of the spheres and A is a phenomenological parameter, whose value ranges between 0.1 and 1.5, depending on the theories describing the plasmon resonance in a particle and the scattering of the electrons by the surface of the particles.[5] Formulas have been proposed in the literature for particles with specific shapes, such as spheroids, where R is replaced by an effective length L_{eff}.[28] In the case of oblate spheroids, L_{eff} is between $4/3c$ for a sphere and $8/3c$ for an extremely flat spheroid, where c is the half-axis of the spheroid along the revolution axis (Figure 1a). For the samples investigated here, the height $2c$ of most of the particles is between 3 to 10 nm (see Part 4 and Figure 4). With a value of A taken equal to 1, this leads to values of $l_{mod}{}^{-1}$ lying approximately between 0.1 and 0.5 nm^{-1}. This increase of $l_{mod}{}^{-1}$ with respect to the bulk value (0.02 nm^{-1}) leads to a so-called homogeneous broadening of the plasmon resonance for a single Ag NP, as shown in Figure 6. The extinction spectra of an oblate spheroid with an aspect ratio equal to 4.5 embedded in amorphous carbon is drawn using the bulk dielectric function of Ag and the modified one with $l_{mod}{}^{-1}$ = 0.2 nm^{-1}. The broadening is much smaller than the experimental width of the resonance for the Ag particles in carbon, which will be discussed below. To get a broadening as large as the one experimentally measured, a value of $l_{mod}{}^{-1}$ equal to 1.7 nm^{-1} would be necessary, that is, an effective mean free path l_{mod} equal to 0.6 nm, which is nonphysical for particles whose smaller size is between 3 and 10 nm. Consequently, the experimental broadening is to be explained by the extrinsic (or inhomogeneous) broadening due to the dispersion of shapes of the NPs in the actual sample. The exact value of $l_{mod}{}^{-1}$ that has to be considered for a single Ag NP is therefore not a crucial point here, as the homogeneous broadening is much smaller than the inhomogeneous one, and will be taken in the following to be equal to 0.2 nm^{-1} for every particle.

As for the films of evaporated carbon, we use the dielectric function of amorphous carbon determined in our laboratory by ellipsometry.[29]

3.2. Spherical DA. The optical response of an isolated ellipsoidal metal NP embedded in a matrix of dielectric function ε_m can be described, in the quasi-static approximation, valid for sizes much smaller than the wavelength of light, by a point dipole, whose induced dipole moment $\vec{p}$ is related to the external electric field $\vec{E}^{ext}$ in S.I. units by

$$\vec{p} = \varepsilon_m\varepsilon_o\alpha\,\vec{E}^{ext} \quad (4)$$

Here ε_o is the vacuum permittivity, and α is the polarizability tensor of the particles, whose diagonal components along the three main axes are given by[30,31]

$$\alpha^i = 4\pi abc\frac{1}{3}\cdot\frac{\varepsilon - \varepsilon_m}{\varepsilon_m + (\varepsilon - \varepsilon_m)L_i} \quad (5)$$

dx.doi.org/10.1021/jp1056495 |J. Phys. Chem. C 2011, 115, 2914–2922

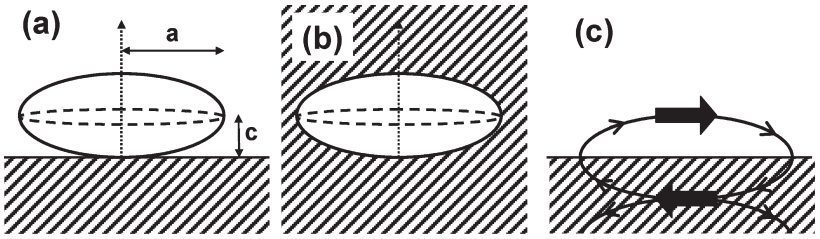

Figure 1. (a) Scheme of a Ag oblate spheroid supported on the carbon substrate. (b) Ag spheroid embedded in carbon. (c) Scheme of the spheroid modeled as a point dipole, in interaction with is own image-dipole in the carbon substrate.

where a, b, and c are the half-axes of the ellipsoid, ε is the frequency-dependent dielectric function of the metal, and L_i is the depolarization factor of the ellipsoid in direction i,[9,30,31] whose values range between 0 and 1. For oblate (i.e., flat) spheroids with the (short) revolution axis along z, they read

$$L_{x,y} = (1+\xi_0^2)\left\{-\frac{1}{2}\frac{\xi_0^2}{1+\xi_0^2}+\frac{1}{2}\xi_0 \arctan\left(\frac{1}{\xi_0}\right)\right\} \quad (6)$$

$$L_z = (1+\xi_0^2)\left\{1-\xi_0 \cdot \arctan\left(\frac{1}{\xi_0}\right)\right\} \quad (7)$$

where $\xi_0 = 1/(r^2-1)^{1/2}$ is a function of the aspect ratio ($r = a/c$) of the particles (see Figure 1). These two depolarization factors are drawn in Figure 2 in blue lines (curves 1), ranging from 1/3 for a sphere ($r = 1$) to 0 and 1, respectively, for an infinitely flat particle ($1/r = 0$).

The plasmon resonances of the metal spheroids are given by the poles of its polarizability, and therefore by $\mathrm{Re}(\varepsilon/\varepsilon_m) = 1 - [1/L_i]$. For a sphere ($L_i = 1/3$), the plasmon resonance can be written by the well-known expression $\mathrm{Re}(\varepsilon/\varepsilon_m) = -2$. For an oblate spheroid with the polarization of light along the long axes, $L_i = L_{x,y}$ is smaller than 1/3, and the plasmon resonance is obtained for more negative values of $\mathrm{Re}(\varepsilon/\varepsilon_m)$, and thus for longer wavelengths. This is illustrated in Figure 3b and 3c, where the extinction spectra of isolated Ag oblate spheroids of different aspect ratios are drawn (solid lines) and compared to the position for a sphere. Keeping in mind that the polarization of light is along the long axes (x or y), the position of the plasmon resonances shifts to longer wavelengths with the increase of the aspect ratio r. The situation is modified when the spheroid is in interaction with a substrate. The multipole method based on an infinite series of spherical multipoles, which solves exactly the interaction of a small spherical or spheroidal particle above a flat substrate, reduces at first order to what is usually called the dipole approximation, and which will be called here, following Bobbert and Vlieger, the spherical DA.[9] This approach was first developed by Yamaguchi et al.[14] as early as 1974 and has been discussed in detail more recently by Pinchuk et al.:[15] considering that the center of the particle is located above a substrate at the distance d, the interaction of the polarized metal ellipsoid with the substrate can be described, within the quasistatic image model, in terms of image charges within the substrate,[14,15,32] via the image-factor $F = (\varepsilon_s - \varepsilon_m)/(\varepsilon_s + \varepsilon_m)$, where ε_s is the frequency-dependent dielectric function of the substrate. In this first-order approximation, the ellipsoid and its image can still be described by interacting point-dipoles. The electric field radiated by the image-dipole therefore modifies the electric field acting on the given particle above the surface, as schematized in Figure 1c. This leads to an effective polarizability whose expression is given by

$$\tilde{\alpha}^{x,y} = \frac{\alpha^{x,y}}{1-F\dfrac{\alpha^{x,y}}{32\pi d^3}} \quad (8)$$

for polarizations parallel to the substrate, and

$$\tilde{\alpha}^{z} = \frac{\alpha^{z}}{1-F\dfrac{\alpha^{z}}{16\pi d^3}} \quad (9)$$

for the polarization perpendicular to the substrate. If the particle is in contact with the substrate, then $d = c$ (Figure 1a). For particles in vacuum or in air ($\varepsilon_m = 1$) supported on a substrate, the factor F is a positive quantity, except in some narrow frequency ranges for substrates displaying resonances (when $-1 < \varepsilon_s < 1$). With $F > 0$, the electric field radiated by the image-dipole, for the polarization of light both parallel and perpendicular to the substrate, decreases the restoring force acting on the free electrons of the particle, leading to a decrease of the resonance frequency, and therefore an increase of the wavelength of the plasmon resonance or "red-shift" (Figure 1c).[32] Combining eq 5 with eqs 8 and 9, the effective polarizability of the particle can be expressed as follows:

$$\tilde{\alpha}^{i} = 4\pi abc\frac{1}{3}\cdot\frac{\varepsilon-\varepsilon_m}{\varepsilon_m+(\varepsilon-\varepsilon_m)\tilde{L}_i} \quad (10)$$

where $\tilde{L}_i$ are the effective depolarization factors, given by[14,15]

$$\tilde{L}_{x,y} = L_{x,y} - \frac{1}{24}\frac{abc}{d^3}F \quad (11)$$

$$\tilde{L}_{z} = L_{z} - \frac{1}{12}\frac{abc}{d^3}F \quad (12)$$

The resonance is obtained for the pole of the polarizability, i.e., for $(\varepsilon/\varepsilon_m) = 1 - (1/\tilde{L}_i)$. As an example, for a sphere in air ($\varepsilon_m = 1$) in contact with the substrate ($a = b = c = d$), and with an image factor F equal to 1 (case of a substrate with high index of refraction), $\tilde{L}_{x,y} = 0.29$ and $\tilde{L}_z = 0.25$ instead of 1/3 obtained for an isolated sphere. This induces both a splitting and a red-shift of the plasmon resonance. In this case of spheres, the modification is rather small, and this spherical DA approach gives results in good agreement with experiments, as it has been shown recently by Pinchuk et al.[15]

On the contrary, for flat particles on a substrate, the quantity abc/d^3 in eqs 11 and 12 becomes large (for instance, it reaches a value of 4 for an oblate spheroid with an aspect ratio $r = a/c$

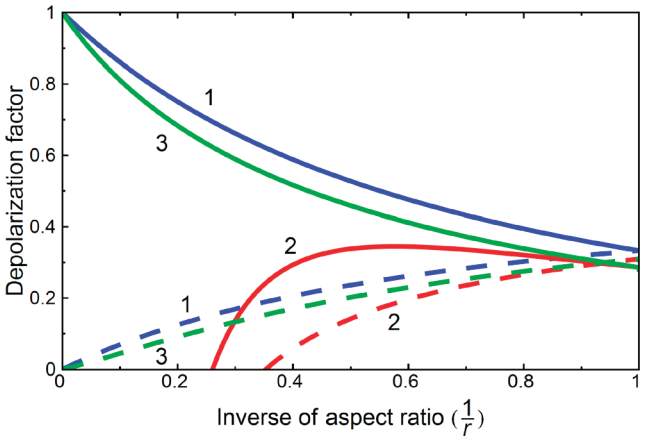

Figure 2. Blue lines (curves 1): depolarization factors of isolated oblate particles; red lines (curves 2): depolarization factors (real part) for supported particles in the spherical DA; green lines (curves 3): depolarization factors (real part) for supported particles in the spheroidal DA. Solid lines refer to polarization of light along the short revolution axis z, while dashed lines refer to polarization of light along the long axes x and y.

equal to 2), leading to very large modifications of the effective depolarization factors. $\tilde{L}_{x,y}$ and $\tilde{L}_z$ calculated in the spherical DA for Ag NPs upon a carbon substrate are drawn in Figure 2 in red lines (curves 2). They decrease quickly with $1/r$, which, when translated in terms of the position of the plasmon resonances, leads to large red-shifts of the resonances, as is shown in Figure 3a (dashed lines). Eventually, when the spheroids are still flatter ($1/r$ < 0.35 and 0.26, respectively) the values of $\tilde{L}_{x,y}$ and $\tilde{L}_z$ become negative, which leads to the disappearance of the plasmon resonances. Such consequence of the use of the spherical DA had been shown previously by Vlieger's group.[9,18] The overestimation of the interaction with the substrate in the spherical DA, and therefore of the red shift of the plasmon resonance, is due to the fact that the distance between the dipole and the image-dipole is small for flat particles. This leads, in this DA, to a very strongly overestimated electrostatic interaction between them, which would be reduced by taking into account the complete series of multipoles in the usual (spherical) space coordinates.

3.3. Spheroidal Dipolar and Quadrupolar Approximations. In order to overcome the problem, Bobbert and Vlieger[9,18] developed a similar model, where the Maxwell equations describing the particle/substrate system were solved within spheroidal coordinates, according to the shape of the considered spheroidal particle. This approach can be used for oblate or prolate spheroids, but it is restricted to the revolution axis normal to the substrate. This leads to an infinite series of *spheroidal* multipoles, which also reproduces the actual charge distribution at the surface of the particles. The authors showed that the calculation of the polarizability of the particles converges much more rapidly than by using the spherical coordinates, and that "even the dipole approximation (the first order approximation) already gives a quite good result".[9] This will be called in the following the spheroidal DA.

In the spheroidal DA, the expression of the polarizability is given by

$$\tilde{\alpha}^{*i} = 4\pi abc\frac{1}{3}\cdot\frac{\varepsilon-\varepsilon_m}{\varepsilon_m+(\varepsilon-\varepsilon_m)\tilde{L}_i^*} \qquad (13)$$

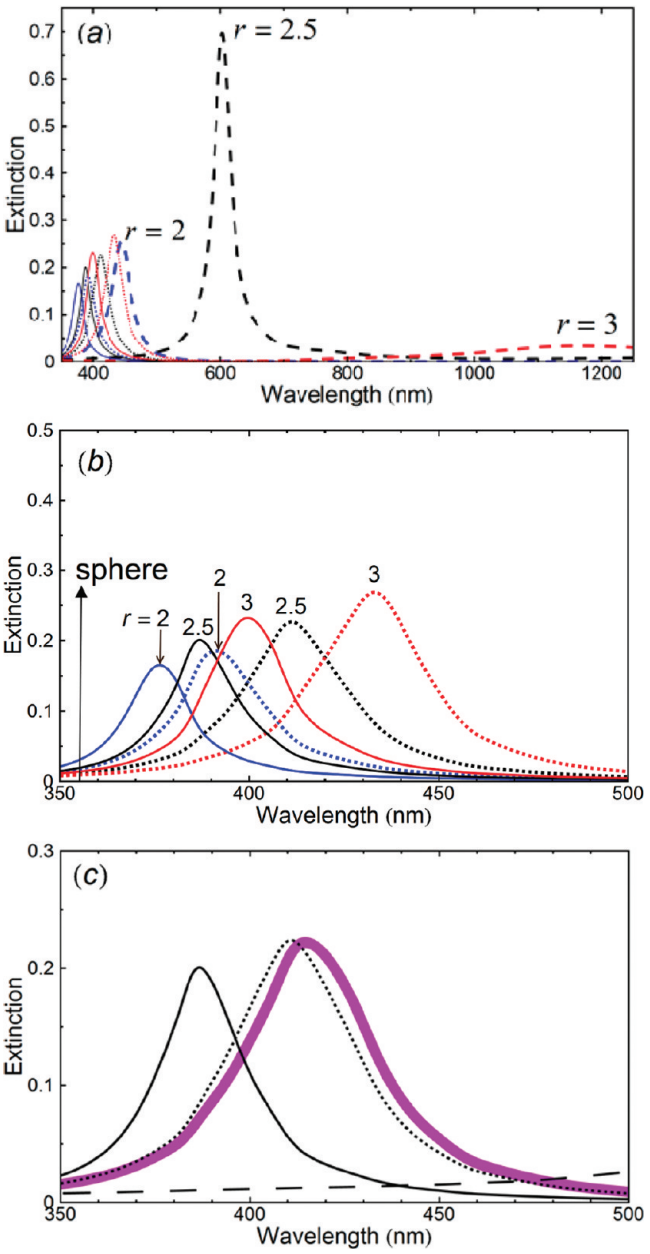

Figure 3. Extinction spectra for polarization of light along the long axes of Ag oblate spheroids with different aspect ratios supported on carbon substrate. (a) Full range. (b) Zoom between 350 and 500 nm. Solid lines: isolated particles in air without interaction with the substrate; dashed lines: spherical DA; dotted lines: spheroidal DA. The aspect ratios r = 2 (blue lines), 2.5 (black lines), and 3 (red lines) are indicated in the figure. The position for an isolated sphere in air is given for comparison in panel b. (c) Comparison between the spherical DA (black dashed line), the spheroidal DA (black dotted line), the spheroidal quadrupolar approximation (violet solid thick line), and the isolated particle (black solid thin line) for r = 2.5.

where $\tilde{L}_i^*$ are the effective depolarization factors, given for oblate spheroids (different expressions are obtained for prolate ones) by

$$\tilde{L}_{x,y}^* = L_{x,y} + \frac{1}{2}F(1+\xi_0^2)\left\{\left(\frac{3}{2}+\xi_0^2\right)\xi_0^2\ln\left(1+\frac{1}{\xi_0^2}\right) - \xi_0\,\mathrm{atan}\left(\frac{1}{\xi_0}\right) - \xi_0^2\right\} \qquad (14)$$

dx.doi.org/10.1021/jp1056495 |J. Phys. Chem. C 2011, 115, 2914–2922

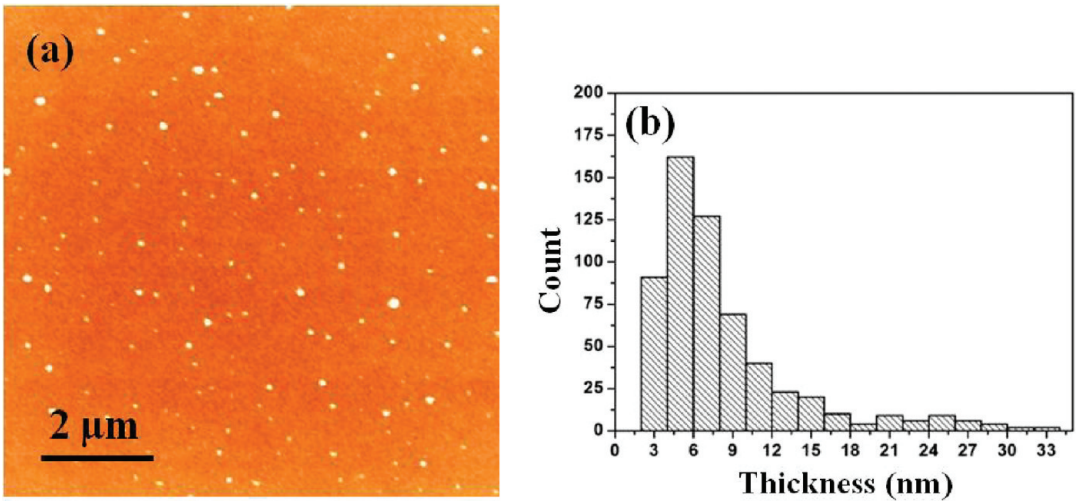

Figure 4. (a) AFM image (10 μm × 10 μm) of the silver NPs on the carbon substrate. (b) Height distribution.

$$\tilde{L}_z^* = L_z + F(1+\xi_0^2)\left\{\left(\frac{3}{2}+\xi_0^2\right)\xi_0^2 \ln\left(1+\frac{1}{\xi_0^2}\right) - \xi_0 \operatorname{atan}\left(\frac{1}{\xi_0}\right) - \xi_0^2\right\} \quad (15)$$

They are drawn in Figure 2 in green lines (curves 3) as a function of $1/r$ and are compared to the case of an isolated particle and to the spherical DA. For a supported sphere ($1/r$ = 1), both DA approximations give of course the same result, which is not very different from the one of the isolated sphere. As the particle becomes flatter (decreasing $1/r$) the difference between both approximations increases. Contrarily to the spherical DA, the values of the effective depolarization factors $\tilde{L}_{x,y}^*$ and $\tilde{L}_z^*$ in the spheroidal DA are close to the depolarization factors $L_{x,y}$ and L_z of the isolated particle. The corresponding extinction spectra are shown in Figure 3 (dotted lines), and their positions are only slightly red-shifted with respect to the ones of the isolated particles (e.g., shift of 15 nm for r = 2 and of 33 nm for r = 3). This shows that the influence of the substrate on the plasmon resonance of a supported particle is actually not large, whatever the flatness of the particle is. It is definitely smaller than the one obtained in the conventional spherical DA.

In order to check that the spheroidal DA gives a satisfactory results, as stated by Bobbert and Vlieger, we draw in Figure3c the extinction spectrum for an oblate spheroid with an aspect ratio equal to 2.5, calculated by use of the spheroidal quadrupole approximation, for which Bedeaux and Vlieger also proposed analytical expressions in ref 18, including four different effective depolarization factors. It is compared to the spherical DA, the spheroidal DA, and to the case of an isolated particle. In the spherical DA, the plasmon resonance is located at 600 nm (Figure 3a), while it is shifted to 410 nm in the spheroidal DA. In the spheroidal quadrupole approximation, this latter position is very weakly shifted by about 5 nm and is not enlarged. This confirms that the spheroidal DA provides a satisfactory model for taking into account the electrostatic interaction between a spheroidal particle with a substrate, and it will be used in the following. It also shows that the large experimental width of the resonance (Figure 6) is not due to some multipolar effect.

4. EXPERIMENTAL RESULTS AND DISCUSSION

Figure 4a shows an AFM image of the sample with uncovered Ag NPs. The distribution of the heights of the NPs, measured over five images of 10 μm × 10 μm, is shown in Figure 4b. Most of the NPs have heights between 3 and 10 nm, with an average of 8 nm. These AFM results also show a lateral size of the NPs larger than their height. The measurement performed on a typical particle of height 8 nm (Figure 5a) shows an apparent lateral size of 60 nm. Because of the convolution between the shape of the particle and the one of the AFM tip, the measured lateral size is larger than the real one. With a typical curvature radius of the tips used in our AFM, determined to be about 10 nm,[33] the lateral size of this Ag NP is about 40 nm, indicating that it has an oblate shape, described by c = 4 nm and $a = b$ = 20 nm, and therefore an aspect ratio around 5. Figures 4 and 5 also show that the distances between the particles are large, resulting in negligible interactions between particles that consequently will not be considered in the present study.

The experimental extinction spectra are drawn in solid lines for both samples in Figure 6. They display broad resonance bands, typical of plasmon resonances in the Ag NPs, centered at 690 nm for the NPs embedded in amorphous carbon and at 500 nm for the uncovered Ag NPs. The large width of the resonance is likely due to the dispersion of shapes of the NPs, in agreement with the dispersion of NP heights c displayed by the AFM measurements (Figure 4b). The positions of the plasmon resonance are at much longer wavelengths than the ones calculated for a Ag sphere in a carbon matrix or supported on a carbon film in the dipolar approximation, located at 475 and 360 nm, respectively (see the arrows drawn in Figure 6). The longer wavelengths of the resonances, with the polarization of light parallel to the carbon film, are expected because of the flattened shapes of the particles, as shown by the AFM measurements. In the used geometry, only the plasmon resonance parallel to the long axes x and y of the NPs is probed. Although it is likely that all the particles do not have a perfectly regular shape, for simplicity, we will model them as oblate spheroids ($a = b > c$), lying on the amorphous carbon surface with their short revolution axis perpendicular to the substrate, or embedded with the same orientation in the carbon film.

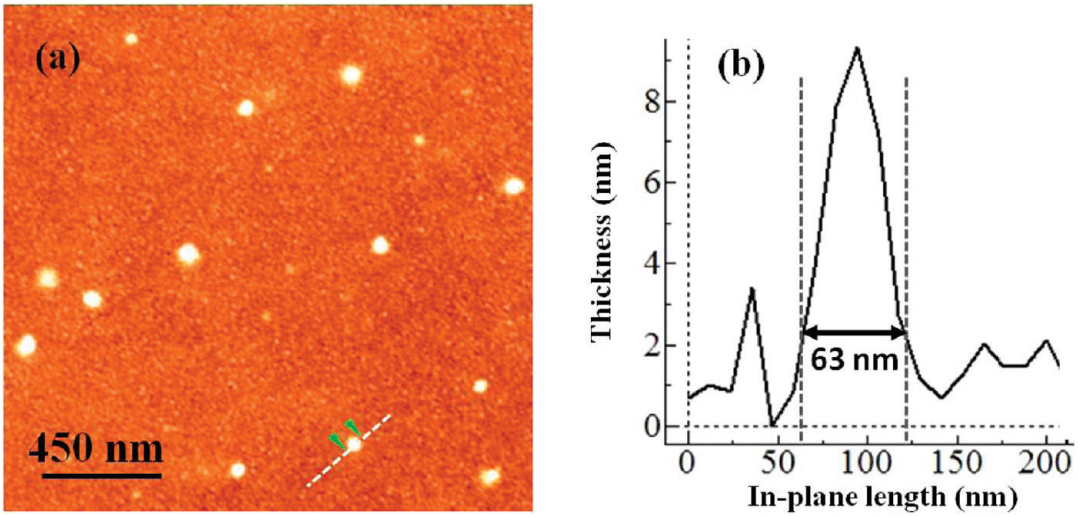

Figure 5. (a) Zoom of the AFM image. (b) Measured profile of a typical 8 nm thick particle.

The extinction cross-section for small NPs in a medium is defined by

$$C_{ext} = \frac{\lambda^2}{\pi} \mathrm{Re}\left\{\frac{S(0°)}{\varepsilon_m}\right\} \quad (16)$$

where $S(0°)$ is the scattering amplitude in the forward direction,[34,35] which reduces at first order in the size of the particle (quasi-static approximation) to

$$C_{ext} = \frac{2\pi}{\lambda} \mathrm{Im}\{\sqrt{\varepsilon_m}\alpha\} \quad (17)$$

where α is the polarizability of the particle, given by one of the above equations, depending on the chosen model, and ε_m is the complex dielectric function of the embedding medium, taken here to be equal to 1 for the particles in air, or equal to the dielectric function of carbon for the embedded particles.

We first use this expression for calculating the extinction of a Ag NP embedded in amorphous carbon. In order to obtain the maximum of the resonance located at 690 nm as in the experimental spectrum, the aspect ratio of the NP had to be taken equal to 4.5, close to the one determined on the typical Ag NP shown in Figure 5. The spectrum calculated for a nominal Ag thickness of 2 nm (the same as for the experimental spectrum) is drawn as a dashed curve in Figure 6a. The intensity of the calculated spectrum has been reduced by a factor of 5. It displays an intensity larger and a width smaller than the measured ones, because the distribution of shapes in the real sample has not been taken into account in this calculation. With the same aspect ratio of 4.5 and the same Ag thickness, we calculate now the extinction spectra, still reduced by a factor 5, for an isolated particle in air, and for a particle supported on the carbon film, by using the two previously described approximations. The results are compared to the spectrum measured for the sample with the Ag NPs supported on a carbon film (Figure 6b). The extinction for the isolated Ag NP with $r = 4.5$ (red dotted line) has a maximum at 440 nm, i.e., at a shorter wavelength than the experimental maximum. This shows again that the main effect of the substrate is to induce a small red-shift of the plasmon resonance. The extinction spectra for the supported NP are strongly dependent on the used model. In the case of the spherical DA, based on eq 8, the spectrum does not display any plasmon resonance, and its intensity is so small in the investigated wavelength range that it is mixed up with the horizontal axis of Figure 6b. The disappearance of the plasmon resonance in the spherical DA for a flat particle was expected from Figure 2, which showed that the effective depolarization factor $\tilde{L}_{x,y}$ becomes negative for large aspect ratio r. On the contrary, the spheroidal DA leads to the extinction spectrum drawn in Figure 6b as a blue dashed line, which displays a maximum located at 490 nm, very close to the observed plasmon resonance maximum at 500 nm.

These results clearly show that, for a flat particle on a substrate, the conventional spherical DA completely fails to reproduce the experiment, because it strongly overestimates the interaction of the particle with the substrate. The real interaction of the particle with the substrate is therefore much smaller that the one considered in the conventional spherical model. On the contrary, the spheroidal DA appears to give a good estimation of the actual red-shift of the resonance induced by the interaction with the substrate. It can be noticed that this red-shift with respect to the plasmon of the isolated particle, although not negligible (here, about 50 nm), is not very large, and that neglecting the interaction with the substrate would remain a better approximation for flat particles than using the conventional spherical DA.

In a second step, the distribution of shapes of the NPs in the sample is considered. We now fit the experimental spectrum for Ag NPs embedded in amorphous carbon, by determining an appropriate distribution of aspect ratios. As performed successfully for other systems of NPs,[36,37] we determined an *ad hoc* distribution of aspect ratios whose weights are adjusted in order to reproduce the experimental spectrum. Because the NP cross-section is proportional to the NP volume divided by the wavelength, the weights correspond to the total volume of NPs per unit surface, associated with one given aspect ratio. They consequently correspond to the equivalent Ag thickness associated with the corresponding aspect ratio. The colored curves in Figure 7a correspond to the extinction spectra of the embedded particles for the different aspect ratios considered in this distribution. The dashed curve drawn in Figure 7a is the result of the sum of all these extinction spectra and, because of the way the distribution of shapes has been built, it perfectly reproduces the experimental spectrum for wavelengths longer than 470 nm. The nominal thickness including all the aspect ratios is found to be 1.66 nm, very close to the actual deposited thickness (2 nm). This slightly smaller value is likely due to the fact

dx.doi.org/10.1021/jp1056495 |*J. Phys. Chem. C* 2011, 115, 2914–2922

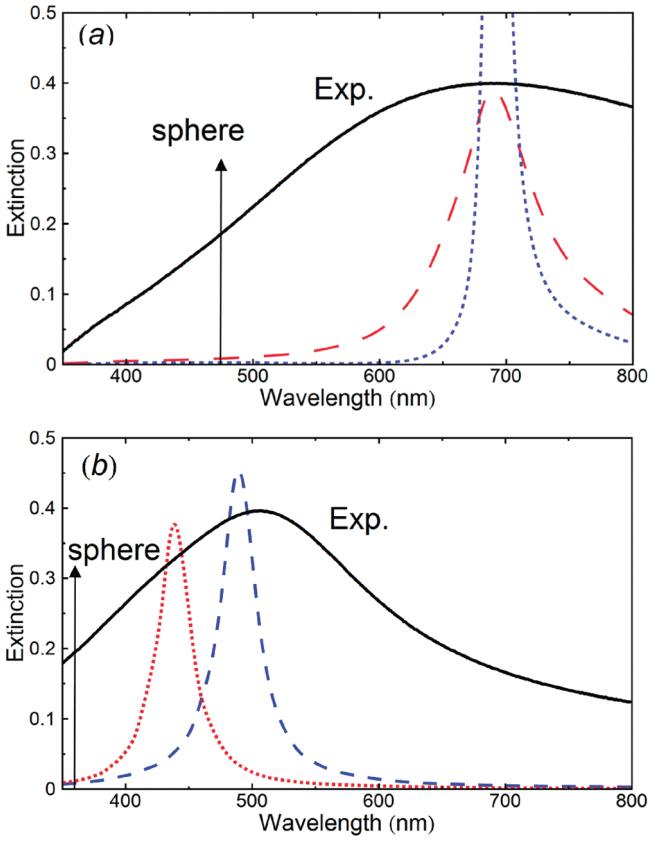

Figure 6. (a) Experimental extinction spectrum of the Ag nanoparticles embedded in the carbon matrix (black solid line) and theoretical spectra, reduced by a factor 5, for embedded NPs with aspect ratio $r = 4.5$ (blue dotted line: calculation using bulk dielectric function of Ag; red dashed line: calculation using modified dielectric function, with $l_{mod}^{-1} = 0.2\ nm^{-1}$); the arrow corresponds to the position for an embedded sphere. (b) Experimental extinction spectrum of the supported Ag NPs (black solid line) and theoretical spectra, reduced by a factor 5, for the Ag NPs with aspect ratio $r = 4.5$, without interaction with the substrate (red dotted line), in the spherical DA (line superposed with the x axis), and in the spheroidal DA (dashed blue line); the arrow corresponds to the position for an isolated sphere in air.

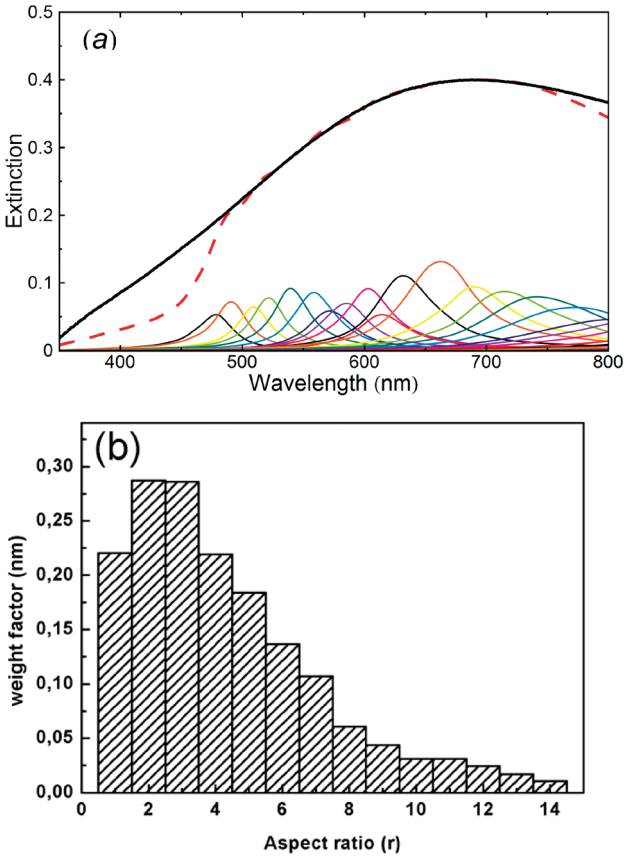

Figure 7. (a) Black solid line: experimental extinction spectrum of the particles inside the carbon matrix; colored solid lines: theoretical spectra corresponding to each different aspect ratio; red dashed line: theoretical spectrum for the distribution of shapes (sum of the individual spectra). (b) Distribution of the aspect ratios r corresponding to panel a.

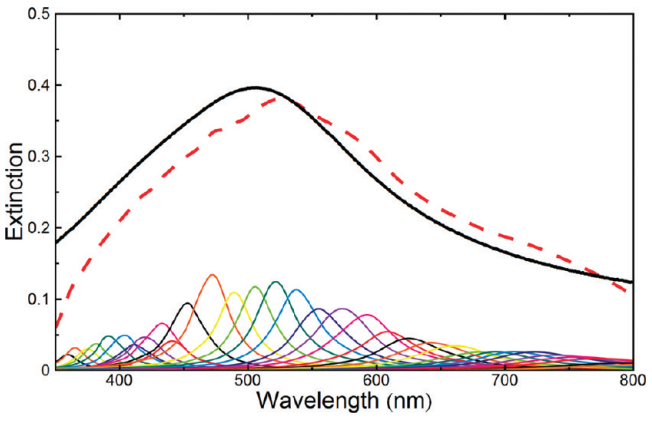

Figure 8. Black solid line: experimental extinction spectrum of the supported particles; colored solid lines: theoretical spectra corresponding to each different aspect ratio calculated in the spheroidal DA; red dashed line: theoretical spectrum for the distribution of shapes (sum of the individual spectra).

that particles giving rise to plasmon resonances at wavelengths smaller than 470 nm and larger than 800 nm are not considered in the present calculation. The corresponding shape distribution is shown in Figure 7b, and the average aspect ratio is $r_{av} = 4.3$. The difference between the experimental curve and the simulated one for wavelengths smaller than 470 nm could be due to the presence of small particles with diameters less than 5 nm, for which the quantum size effect leading to a spilling out of the free electron distribution at the surface, might be important.[38,39] Such effect is known indeed to induce a blue shift of the resonance for silver small particles, and would increase the observed extinction for short wavelengths. This effect could have been considered by adding a given amount of particles with *ad hoc* dielectric functions, in order to account for this quantum size effect, but for simplicity this has not been done here.

Now, we use this so-determined distribution of aspect ratios to calculate the extinction spectrum of the sample with the uncovered particles lying on the carbon film, within the spheroidal DA. The colored curves in Figure 8 are the extinction spectra for each individual shape. The dashed curve, which is the sum of all the individual curves, appears to be in very good agreement both in shape and in intensity with the experimental one. The only difference is a slightly red-shift of 25 nm of the calculated curve. This shows clearly that the spheroidal DA is a very efficient approximation to describe the optical response of a supported flat metal NP. Moreover, this suggests that the previously determined

distribution of NPs aspect ratios is close to the real one. On the one hand, it must be underlined anyway that this shape distribution, issued from optical measurements cannot exactly reproduce the real shape distribution. Ag NPs are expected to be truncated particles, which are represented here by spheroids for the analytic calculation of their optical extinction. It is not obvious in particular that the aspect ratios obtained through the analysis of optical spectra closely correspond to the exact aspect ratios of truncated spheres. On the other hand the small remaining discrepancy observed in Figure 8 could be due to the fact that both samples, although prepared in identical conditions, could differ a little in the actual distribution of shapes of the Ag NPs. Some modification of the supported Ag NPs could also occur when exposed to air, with respect to the carbon-protected ones, or could on the contrary be induced by the additional carbon layer in the embedded-NP sample. It is also possible that the dielectric function of amorphous carbon used in the calculation does not perfectly describe the optical response of our samples.

5. CONCLUSION

The experimental optical extinction of an assembly of Ag NPs with flat shapes, lying upon a carbon film, is compared to results of calculation by use of different models. It is shown that the conventional "spherical" dipolar model, which describes the interaction of a particle with the substrate in terms of a point-dipole interacting with its own image-dipole, completely fails to reproduce the observed plasmon resonance of the supported particles. The failure of this model is due to the fact that the distance between the dipole and the image-dipole is small for flat particles, leading to a very important overestimation of their mutual interaction. On the contrary, the use of the "spheroidal" dipolar model, resulting also in an easy-to-use formula, leads to a very good agreement with the experiment. These results reveal that the effect of the surface on the plasmon resonance for flat particles is a red-shift of about the same importance as the one for spheres, in strong contrast with the conventional spherical DA. Consequently, we would like to encourage future works dealing with the optical properties of supported flat particles to use this spheroidal DA. We evidence how the use of spheroidal DA allows one to determine the distribution of NPs adsorbed on a substrate, even for flat NPs in interaction with the substrate. It would be interesting now to check these effects for other systems, such as metal nanorods on a surface, but to our knowledge, no simple model has been developed for this latter system. Nevertheless, it appears reasonable to extrapolate these results and to think that the conventional approach should also fail, as the distance between the particle and its self-image is reduced for elongated nanorods. In this case, effective depolarization factors for lying prolate spheroids would likely be only a little smaller than the depolarization factors of isolated spheroids. In this last system, in order to get rid of the inhomogeneous broadening of the plasmon resonance due to the dispersion of shapes of the NPs, measurements performed at the single particle level, using, for instance, photothermal spectral microscopy,[40] would allow one to reach a better comparison between experiment and theory.

AUTHOR INFORMATION

Corresponding Author

*E-mail: yves.borensztein@insp.jussieu.fr (Y.B.), emmanuelle.lacaze@insp.jussieu.fr (E.L.).

ACKNOWLEDGMENT

We acknowledge fruitful and illuminating discussions with Ruben Barrera.

REFERENCES

(1) Barnes, W. L.; Dereux, A.; Ebbesen, T. W. *Nature* **2003**, *424*, 824.
(2) Anker, J. N.; Hall, W. P.; Lyandres, O.; Shah, N. C.; Zhao, J.; Van Duyne, R. P. *Nat. Mater.* **2008**, *7*, 442.
(3) Larsson, E. M.; Langhammer, C.; Zoric, I.; Kasemo, B. *Science* **2009**, *326*, 1091.
(4) Zijlstra, P.; Chon, J. W. M.; Gu, M. *Nature* **2009**, *459*, 410.
(5) Kreibig, U.; Vollmer, M. *Optical Properties of Metal Clusters*; Springer: New York, 1994.
(6) Myroshnychenko, V.; Rodriguez-Fernandez, J.; Pastoriza-Santos, I.; Funston, A. M.; Novo, C.; Mulvaney, P.; Liz-Marzan, L. M.; de Abajo, F. J. G. *Chem. Soc. Rev.* **2008**, *37*, 1792.
(7) Sosa, I. O.; Noguez, C.; Barrera, R. G. *J. Phys. Chem. B* **2003**, *107*, 6269.
(8) Bobbert, P. A.; Vlieger, J. *Physica A* **1986**, *137*, 209.
(9) Bobbert, P. A.; Vlieger, J. *Physica A* **1987**, *147*, 115.
(10) Roman-Velazquez, C. E.; Noguez, C.; Barrera, R. G. *Phys. Rev. B* **2000**, *61*, 10427.
(11) Jain, P. K.; El-Sayed, M. A. *Chem. Phys. Lett.* **2010**, *487*, 153.
(12) Romero, I.; Aizpurua, J.; Bryant, G. W.; de Abajo, F. J. G. *Opt. Exp.* **2006**, *14*, 9988.
(13) Kelly, K. L.; Coronado, E.; Zhao, L. L.; Schatz, G. C. *J. Phys. Chem. B* **2003**, *107*, 668.
(14) Yamaguchi, T.; Yoshida, S.; Kinbara, A. *Thin Sol. Films* **1974**, *21*, 173.
(15) Pinchuk, A.; Hilger, A.; von Plessen, G.; Kreibig, U. *Nanotechnology* **2004**, *15*, 1890.
(16) Camelio, S.; Babonneau, D.; Lantiat, D.; Simonot, L.; Pailloux, F. *Phys. Rev. B* **2009**, 80.
(17) Witkowski, N.; Borensztein, Y.; Baudot, G.; Repain, V.; Girard, Y.; Rousset, S. *Phys. Rev. B* **2004**, *70*, 085408.
(18) Bedeaux, D.; Vlieger, J. *Optical Properties of Surfaces*; Imperial College Press: London, 2004.
(19) Beitia, C.; Borensztein, Y.; Lazzari, R.; Nieto, J.; Barrera, R. G. *Phys. Rev. B* **1999**, *60*, 6018.
(20) Lazzari, R.; Renaud, G.; Revenant, C.; Jupille, J.; Borensztein, Y. *Phys. Rev. B* **2009**, 79.
(21) Ruppin, R. *Sur. Sci.* **1983**, *127*, 108.
(22) Stefanou, N.; Modinos, A. *J. Phys.: Condens. Matter* **1991**, *3*, 8135.
(23) Lazzari, R.; Jupille, J.; Borensztein, Y. *Appl. Surf. Sci.* **1999**, *142*, 451.
(24) Johnson, P. B.; Christy, R. W. *Phys. Rev. B* **1972**, *6*, 4370.
(25) Borensztein, Y.; Alameh, R.; Roy, M. *Phys. Rev. B* **1994**, *50*, 1973.
(26) Martin, D.; Jupille, J.; Borensztein, Y. *Surf. Sci.* **1998**, *402*, 433.
(27) Hovel, H.; Fritz, S.; Hilger, A.; Kreibig, U.; Vollmer, M. *Phys. Rev. B* **1993**, *48*, 18178.
(28) Coronado, E. A.; Schatz, G. C. *J. Chem. Phys.* **2003**, *119*, 3926.
(29) Thèye, M.-L.; Frigerio, J.-M. INSP; Private communication, 2010.
(30) Bohren, C. F.; Huffman, D. R. *Absorption and Scattering of Light by Small Particles*; Wiley: New York, 1998.
(31) Landau, L. D.; Lifshitz, E. M. *Electrodynamic of Continuous Media*; Pergamon Press: New York, 1960.
(32) Barrera, R. G.; Delcastillomussot, M.; Monsivais, G.; Villasenor, P.; Mochan, W. L. *Phys. Rev. B* **1991**, *43*, 13819.
(33) Rodriguez, R. D.; Demaille, D.; Lacaze, E.; Jupille, J.; Chaneac, C.; Jolivet, J. P. *J. Phys. Chem. C* **2007**, *111*, 16866.
(34) Bohren, C. F.; Gilra, D. P. *J. Colloid Interface Sci.* **1979**, *72*, 215.
(35) Videen, G.; Sun, W. B. *Appl. Opt.* **2003**, *42*, 6724.

(36) Eustis, S.; El-Sayed, M. A. *J. Appl. Phys.* **2006**, 100.
(37) Borensztein, Y.; Delannoy, L.; Djedidi, A.; Barrera, R. G.; Louis, C. *J. Phys. Chem. C* **2010**, *114*, 9008.
(38) Borensztein, Y.; Deandres, P.; Monreal, R.; Lopezrios, T.; Flores, F. *Phys. Rev. B* **1986**, *33*, 2828.
(39) Tiggesbaumker, J.; Koller, L.; Meiwesbroer, K. H.; Liebsch, A. *Phys. Rev. A* **1993**, *48*, R1749.
(40) Tchebotareva, A. L.; Ruijgrok, P. V.; Zijlstra, P.; Orrit, M. *Laser Photonics Rev.* **2010**, *4*, 581.